

# Stable solutions of a scalar conservation law for particle-size segregation in dense granular avalanches

M. SHEARER,<sup>1</sup> J. M. N. T. GRAY<sup>2</sup> AND A. R. THORNTON<sup>2</sup>

<sup>1</sup>*Department of Mathematics & Center for Research in Scientific Computation,  
North Carolina State University, Raleigh, NC 27695, USA  
email: shearer@ncsu.edu*

<sup>2</sup>*School of Mathematics & Manchester Centre for Nonlinear Dynamics, University of Manchester,  
Oxford Road, Manchester M13 9PL, UK*

(Received 15 March 2007; revised 29 October 2007)

Dense, dry granular avalanches are very efficient at sorting the larger particles towards the free surface of the flow, and finer grains towards the base, through the combined processes of kinetic sieving and squeeze expulsion. This generates an inversely graded particle-size distribution, which is fundamental to a variety of pattern formation mechanisms, as well as subtle size-mobility feedback effects, leading to the formation of coarse-grained lateral levees that create channels in geophysical flows, enhancing their run-out. In this paper we investigate some of the properties of a recent model [Gray, J. M. N. T. & Thornton, A. R. (2005) A theory for particle size segregation in shallow granular free-surface flows. *Proc. R. Soc.* 461, 1447–1473]; [Thornton, A. R., Gray, J. M. N. T. & Hogg, A. J. (2006) A three-phase mixture theory for particle size segregation in shallow granular free-surface flows. *J. Fluid. Mech.* 550, 1–25] for the segregation of particles of two sizes but the same density in a shear flow typical of shallow avalanches. The model is a scalar conservation law in space and time, for the volume fraction of smaller particles, with non-constant coefficients depending on depth within the avalanche. It is proved that for steady flow from an inlet, complete segregation occurs beyond a certain finite distance down the slope, no matter what the mixture at the inlet. In time-dependent flow, dynamic shock waves can develop; they are interfaces separating different mixes of particles. Shock waves are shown to be stable if and only if there is a greater concentration of large particles above the interface than below. Constructions with shocks and rarefaction waves are demonstrated on a pair of physically relevant initial boundary value problems, in which a region of all small particles is penetrated from the inlet by either a uniform mixture of particles or by a layer of small particles over a layer of large particles. In both cases, and under a linear shear flow, solutions are constructed for all time and shown to have similar structure for all choices of parameters.

## 1 Introduction

The tendency of larger particles to rise towards the surface of gravity-driven avalanches, when the flow regime is dominated by enduring grain–grain contacts, was perhaps first recognised by engineers and geologists [1, 21]. This phenomenon, called inverse- or reverse-grading, occurs in a wide range of natural hazards [7, 9, 12, 25, 31] including debris flows, the dense lower core of pyroclastic flows, lahars, as well as avalanches of sand, rocks and snow. Particle-size segregation also occurs in much smaller-scale granular

avalanches that occur in industrial flows, and can lead to very regular and beautiful patterns in some regimes [5, 33] and complex and irregular behaviour in others [10, 24]. As the grains flow downslope and are sheared over one another the avalanche dilates by about 10%–15% [11]. With increased interstitial pore space the smaller particles tend to percolate downwards, as they are statistically more likely than the larger ones to fit into gaps that open up beneath them. This gravity-driven process is known as kinetic sieving [21] and is combined with squeeze expulsion [26], which generates a return flow of larger particles towards the free surface. Note that in more dilute flows, such as in a powder cloud or a saltation layer, other segregation mechanisms dominate and the direction of segregation may reverse. Geophysicists and hazard planners are becoming increasingly interested in understanding and modelling the evolving grain-size distribution in granular avalanches, because it can have a pronounced feedback on the bulk flow dynamics. In particular, size-mobility feedbacks are responsible for the spontaneous formation of coarse-grained lateral levees, which create channels in the bulk flow and enhance the run-out of hazardous debris and pyroclastic flows [13, 14, 22, 23].

The classic paper of Savage and Lun [26] shows how a single conservation law can describe the segregation of particles of two different sizes in chute flow. The continuum model expresses conservation of mass, with a constitutive law governing the rate of segregation derived from statistical information entropy principles [15]. For the case of a dilute concentration of small particles in a steady fully developed shear flow, Savage and Lun were able to derive approximate solutions that consist of three constant states separated by jumps in concentration. In the real world diffusive remixing of the particles smooths out the discontinuous shocks, but the transition can still be very sharp in slow dry frictional flows. Savage and Lun [26] saw evidence of this along the length of their chute experiment (a photo of which is reproduced in [30]) and used splitter plates to separate and collect samples from a series of different depths and positions in the flow. While their data was not of high enough resolution to explicitly resolve the sharp transitions, it was sufficient to show that their shock solutions were in good quantitative agreement with their experiments [26, 32]. Crucially, their model was able to predict that a bi-disperse mixture would separate out into an inversely graded layer of large particles on top of a layer of fines, sufficiently far downstream.

In this paper, we consider an alternative and simpler continuum model for segregation in a bi-disperse granular avalanche, which was derived in the recent articles of Gray and Thornton [8] and Thornton *et al.* [30] using two- and three-constituent mixture theory. The new model is similar in structure to that of Savage and Lun but it has the virtues of (i) being formulated in terms of the volume fraction of small particles, rather than number density and diameter ratios, which significantly simplifies the theory, and (ii) the normal components of the constituent momentum balances are used to derive the large and small particle percolation velocities, providing a natural way of introducing the gravity dependence of kinetic sieving into the model. In the two-constituent formulation of Gray and Thornton [8] the interstitial pore space is subsumed into the bulk density of the large and small particles. In Thornton *et al.* [30] a fluid is assumed to occupy the pore space. When the fluid density is different from the density of the particles, the model exhibits buoyancy effects similar to those observed experimentally by Vallance and Savage [32]. Both theories assume that the solids volume fraction remains constant to

leading order, which is consistent with particle dynamics simulations [28]. The resulting segregation equation

$$\frac{\partial \phi}{\partial t} + \frac{\partial}{\partial x}(\phi u) + \frac{\partial}{\partial y}(\phi v) + \frac{\partial}{\partial z}(\phi w) - \frac{\partial}{\partial z}(S_r \phi(1 - \phi)) = 0 \quad (1.1)$$

governs the evolution of the volume fraction  $\phi(x, y, z, t)$  of small particles per unit granular volume, as the grains flow down an inclined plane with an imposed incompressible bulk velocity  $(u, v, w)$ . The physical coordinates are defined so that the  $x$ -axis is parallel to the plane, the  $z$ -axis is normal to the plane (with  $z = 0$  marking the plane itself) and  $y$  is the transverse variable. In these theories the volume fraction of large particles per unit granular volume is  $1 - \phi$ . The equation expresses conservation of mass within the mixture, with the final term accounting for the processes of kinetic sieving and squeeze expulsion in the  $z$ -direction and the dimensionless parameter  $S_r$  controlling the segregation rate. Gray and Thornton [8] showed that the  $\phi(1 - \phi)$  structure of the segregation term is exactly the same as the dilute limit of Savage and Lun's [26] theory and the new model can therefore reproduce the quantitative agreement with experiments found by Savage and Lun [26] and Vallance and Savage [32].

Independently, Dolgunin and Ukolov [2] directly postulated the segregation flux in equation (1.1). This was based on the observation that there is no segregation when either the large or the small grains are in a pure phase, so the segregation flux must be zero when either  $\phi = 1$  or  $\phi = 0$ . In their model an additional diffusive term was included on the right-hand side of (1.1) to account for particle remixing in more energetic flows [2, 3]. For energetic time-dependent flows that are independent of  $x$  and  $y$ , the resulting segregation-remixing equation is equivalent to Burgers equation and is subject to non-linear surface and basal no-flux boundary conditions. Gray and Chugunov [3] have constructed general solutions for arbitrary initial conditions by using the Cole–Hopf transformation to linearise the problem. These indicate that the concentration shocks are replaced by smooth transitions that are centred on the shocks and which become increasingly sharp as the relative strength of the remixing decreases. Khakhar *et al.* [16] and Gray and Chugunov [3] have compared the final steady states to the results of particle dynamics simulations [17] and shown that they are in very close agreement with the ‘S’-shaped profiles produced by the theory, for both density- and size-driven segregation. This together with the experimental results of Savage and Lun [26] and Vallance and Savage [32] provide considerable evidence for the form of the segregation flux used in equation (1.1).

The dimensionless segregation number

$$S_r = \frac{LQ}{HU} > 0, \quad (1.2)$$

is defined as the ratio of a typical downstream transport timescale,  $L/U$ , to a typical segregation timescale,  $H/Q$ , where  $H$  and  $L$  are the typical thickness and length of the avalanche,  $U$  is a typical downstream velocity and  $Q/4$  is the maximum segregation velocity of the two species attained at  $\phi = 1/2$ . The three-constituent theory [30] yields the most general form of  $Q = (B/c)\hat{\rho}g \cos \zeta$ , where  $g$  is gravitational acceleration,  $\zeta$  is the chute angle,  $\hat{\rho} = (\rho^{g*} - \rho^{f*})/\rho^{g*}$  is the relative density difference between the grains and

the interstitial fluid and  $c$  is the inter-particle drag coefficient. The model assumes that the small particles support less of the overburden pressure as they percolate downwards, and that the large grains must therefore support the excess load. The dimensionless parameter  $B$  determines how far the constituent pressures deviate away from the lithostatic overburden pressure. While the mixture theory approach provides a natural way of introducing gravity into the theory, it does not provide explicit dependencies of  $S_r$  on the grain-size ratio, the shear rate or the degree of dilation, such as those derived through the statistical mechanics approach of Savage and Lun [26]. Investigations are currently underway to empirically determine the functional dependence of  $S_r$  from laboratory experiments and particle dynamics simulations.

In this paper we consider fully developed bulk flows in which the transverse and normal velocities  $v, w$  are negligible, and the parallel velocity is a specified function  $u = u(z)$  of the depth variable  $z$  only. In these circumstances the avalanche depth is constant, normalised so that  $0 < z < 1$ , and equation (1.1) simplifies to

$$\frac{\partial \phi}{\partial t} + u \frac{\partial \phi}{\partial x} - \frac{\partial}{\partial z}(\phi(1 - \phi)) = 0, \quad (1.3)$$

in which we have scaled the independent variables  $x$  and  $t$  by  $S_r$ , effectively setting  $S_r = 1$ . Equation (1.3) is a non-linear scalar conservation law with a linear depth-dependent flux (in the  $x$ -direction). Our aim is to show how to solve initial boundary value problems for equation (1.3) for typical chute flow configurations in which there is an initial distribution of particles in the semi-infinite domain  $x > 0, 0 < z < 1$ , and an inflow of particles from the left, i.e., at  $x = 0$ . We impose no-flux boundary conditions at the top and bottom of the domain, as no particles cross these parts of the boundary:

$$\phi(\phi - 1) = 0, \quad z = 0, 1. \quad (1.4)$$

Since large particles rise to the surface  $z = 1$  of the flow and small particles descend to the solid inclined plane, this boundary condition can be interpreted as

$$\phi(x, 0, t) = 1; \quad \phi(x, 1, t) = 0. \quad (1.5)$$

However, if there is a region of all large particles adjacent to the lower boundary, then the boundary condition is satisfied due to a horizontal shock along the boundary. Similarly, if there is a region of all small particles adjacent to the upper boundary, then there is a horizontal shock there also. Both shocks are stable, according to hyperbolic theory (see Theorem 4.1).

In Section 2, we recall the method of characteristics as it applies to equation (1.3). The main results of this paper are contained in Sections 3–6. Section 3 contains two main theorems. The first establishes the criterion for the stability of steady shocks as solutions of a scalar conservation law, with the flow direction as time-like. The second result is arguably more significant, as it gives a sharp estimate of the finite distance to full segregation in a steady chute flow or avalanche, independent of the incoming particle mixture. This problem has been addressed in special cases but is resolved here in some generality using the Lax formula for weak entropy solutions of the inviscid Burgers equation. In Section 4, we address the stability of dynamic shocks, showing in Theorem 4.1

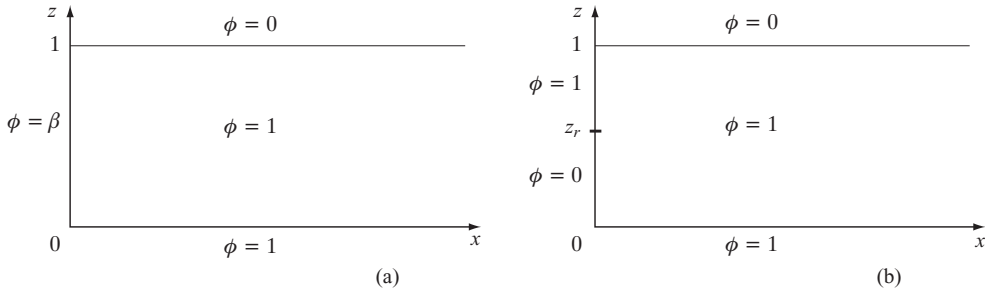


FIGURE 1. Initial and boundary conditions (a) Case I, (b) Case II.

that they are dynamically stable if and only if there is a greater concentration of large particles above the interface than below. We also give a physical explanation of the stability condition. While this result uses standard hyperbolic theory, its significance for particle segregation problems is profound: it predicts that interfaces that break become unstable; the problem of determining the subsequent evolution of a growing mixing zone has only been partially resolved [20]. The theorem has been used by Thornton and Gray [29] to construct breaking segregation waves that are composed of two shocks and two expansions fans, arranged in a ‘lens’-like structure, which travel downslope at constant speed. These lenses are a generic feature of segregation models of this kind and are important for large particle recirculation close to the bouldery margins of geophysical flows [13, 14, 22, 23].

Finally, in Sections 5 and 6, we provide explicit solutions of a pair of initial boundary value problems, complementing explicit solutions of an earlier paper [6]. These are intended to illustrate the behaviour of solutions of the PDE model and how rarefactions and shocks interact to allow large particles to rise above small particles. The solutions also serve as useful prototypes of flow with simple initial and boundary conditions, against which numerical algorithms can be tested. In these problems we assume a linear velocity profile:

$$u = u_x(z) = \alpha + 2(1 - \alpha)z, \quad 0 \leq z \leq 1. \quad (1.6)$$

The parameter  $\alpha$  gives plug flow when  $\alpha = 1$ , simple shear for  $\alpha = 0$  and linear shear with basal slip (at the inclined plane surface) for  $0 < \alpha < 1$ . In contrast to Gray *et al.* [6] we consider an initial particle-size distribution in the chute that consists of small particles only,

$$\phi(x, z, 0) = 1, \quad 0 < x, \quad 0 \leq z \leq 1, \quad (1.7)$$

with two cases of inflow boundary conditions shown in Fig 1, also considered in [6]:

**Case I** Homogeneous mixture inflow:

$$\phi(0, z, t) = \beta, \quad (1.8)$$

where  $0 < \beta < 1$  is a constant.

**Case II** Normally segregated inflow (with small particles above large particles):

$$\phi(0, z, t) = \begin{cases} 0, & z < z_r \\ 1, & z > z_r, \end{cases} \quad (1.9)$$

where  $0 \leq z_r \leq 1$  is a parameter. With the techniques of the earlier sections, we are able to solve these initial boundary value problems explicitly. The construction in case II turns out to be more complicated than that in case I, and the dependence on parameters  $\alpha, z_r$  is more subtle. In principle, it is feasible to construct a laboratory apparatus to generate similar conditions in an experiment. However, direct comparisons with the theory are still some way off, as non-invasive techniques to measure the evolving particle-size distribution are still in their infancy.

## 2 Method of characteristics

Equation (1.3) is a scalar equation in conservation form, so the theory of scalar conservation laws can be applied to construct solutions and to understand their behaviour. The starting point is the method of characteristics, which applies in regions of space-time in which the solution is smooth. Characteristics  $x = x(t)$ ,  $z = z(t)$  are curves along which the solution  $\phi$  is constant. A characteristic curve passing through a point  $(x_0, z_0)$  at time  $t = t_0$  satisfies the system of ordinary differential equations

$$\frac{dx}{dt} = u(z); \quad \frac{dz}{dt} = 2\phi - 1; \quad x(t_0) = x_0; \quad z(t_0) = z_0. \quad (2.1)$$

The system is solved easily for general non-negative  $u(z)$ , since  $t$  may be eliminated:

$$u(z) \frac{dz}{dx} = 2\phi - 1.$$

Since  $\phi$  is constant on characteristics, if we let

$$\psi(z) = \int_0^z u(\zeta) d\zeta, \quad (2.2)$$

we obtain  $x$  as a function of  $z$ :

$$\psi(z) - \psi(z_0) = (2\phi - 1)(x - x_0). \quad (2.3)$$

This gives an equation for  $\phi$  (along each characteristic):

$$\phi(x, z, t) = \frac{1}{2} \left( 1 + \frac{\psi(z) - \psi(z_0)}{(x - x_0)} \right). \quad (2.4)$$

In particular, if we keep  $x_0, z_0$  fixed and allow  $\phi$  to vary in (2.3), we get an *equilibrium rarefaction fan* that is centred on  $(x_0, z_0)$ . In order for the fan to open out for  $x > x_0$ ,  $\phi$  must be increasing with  $z$  (since  $\psi(z)$  is). Thus, the normally segregated inflow boundary condition (1.9) will generate a rarefaction fan centred at  $(0, z_r)$ .

Another special case arises when  $\phi$  is constant on lines  $z = \text{constant}$ , i.e.,  $\phi$  is a function of  $z$  and  $t$  and is independent of  $x$ . From equation (1.3), we find that  $x$ -independent solutions satisfy the equation

$$\frac{\partial \phi}{\partial t} - \frac{\partial}{\partial z}(\phi(1 - \phi)) = 0. \quad (2.5)$$

Returning to the general case of dependence on all three variables,  $x, z, t$ , for the linear shear profile of (1.6), we have

$$\psi(z) = \alpha z + (1 - \alpha)z^2, \quad (2.6)$$

so that characteristics lie on parabolas:

$$x(z) = x_0 + (z - z_0)(\alpha + (1 - \alpha)(z + z_0))/(2\phi - 1). \quad (2.7)$$

It is convenient to relate  $u = u(z)$  directly to  $\psi = \psi(z)$ , eliminating  $z$  between (1.6) and (2.6):

$$u = \sqrt{\alpha^2 + 4(1 - \alpha)\psi}. \quad (2.8)$$

### 3 Steady solutions

Steady solutions satisfy the equation

$$u(z) \frac{\partial \phi}{\partial x} - \frac{\partial}{\partial z}(\phi(1 - \phi)) = 0, \quad x > 0, \quad 0 < z < 1, \quad (3.1)$$

and an inflow boundary condition

$$\phi(0, z) = \phi_0(z), \quad 0 < z < 1, \quad (3.2)$$

in addition to the no-flux boundary conditions (1.5) on the top and bottom  $z = 0, 1$ .

It will be convenient to reduce this problem to the inviscid Burgers equation on the same domain using new variables

$$\tau = x/\psi(1), \quad \zeta = \psi(z)/\psi(1), \quad v = 2\phi - 1.$$

Then (3.1) becomes

$$\frac{\partial v}{\partial \tau} + \frac{\partial}{\partial \zeta} \left( \frac{v^2}{2} \right) = 0, \quad \tau > 0, \quad 0 < \zeta < 1. \quad (3.3)$$

Consider a smooth shock wave, i.e., a  $C^1$  curve  $\zeta = \hat{\zeta}(\tau)$  that separates the plane locally into two components in which the solution  $v(\zeta, \tau)$  is classical:

$$v(\zeta, \tau) = \begin{cases} v_-(\zeta, \tau), & \zeta < \hat{\zeta}(\tau) \\ v_+(\zeta, \tau), & \zeta > \hat{\zeta}(\tau). \end{cases} \quad (3.4)$$

Assuming that  $v$  is piecewise continuous, the Rankine–Hugoniot condition dictates that the shock has speed

$$\hat{\zeta}'(\tau) = \frac{1}{2}(v_+(\hat{\zeta}(\tau), \tau) + v_-(\hat{\zeta}(\tau), \tau)).$$

For steady shocks, we consider  $\tau = x/\psi(1)$  to be a time-like variable (since it increases in the direction of the flow). From this point of view, we can invoke the Lax entropy condition to require that for a shock to be stable there must be a greater concentration of small particles below the shock than above.

**Theorem 3.1** *The shock (3.4) satisfies the Lax entropy condition with  $\tau$  time-like if and only if the shock is inversely graded (large particles above small):*

$$v_+(\hat{\zeta}(\tau), \tau) < v_-(\hat{\zeta}(\tau), \tau). \quad (3.5)$$

More significantly, we can estimate how far from the inlet a steady flow necessarily becomes fully segregated, independent of the inflow condition. A formula for constant inflow conditions was given by Savage and Lun [26], as explained in detail below. In the following theorem, we consider *entropy weak solutions* in the sense of Kruzkov [18, 27]. Since (3.1), (3.2) are posed in a strip rather than a half-plane, weak solutions are defined by extending the problem to  $-\infty < z < \infty$ , letting  $u(z) = u(0), \phi_0(z) = 1$  for  $z < 0$ ,  $u(z) = u(1), \phi_0(z) = 0$  for  $z > 1$ . It is straightforward to check that for a function  $\phi_0 : [0, 1] \rightarrow [0, 1]$  of bounded variation, the weak solution  $\phi(x, z), x \geq 0, -\infty < z < \infty$  of the extended problem has the properties that (almost everywhere)  $\phi(x, z) \in [0, 1]$  and  $\phi(x, z) = 1$  for  $z < 0$ ,  $\phi(x, z) = 0$  for  $z > 1$ .

**Theorem 3.2** *(Steady state segregation) Let  $\phi_0 : [0, 1] \rightarrow \mathbb{R}$  be a function of bounded variation with  $0 \leq \phi_0(z) \leq 1$ . Then the boundary value problem (3.1), (3.2) has a unique entropy weak solution with the property that for some  $x_s \leq 2\psi(1)$  (depending on  $\phi_0$ ), the solution is fully segregated for all  $x > x_s$ :*

$$\phi(x, z) = \begin{cases} 1, & z < z_s \\ 0, & z > z_s \end{cases} \quad \text{for all } x > x_s. \quad (3.6)$$

Moreover,  $z_s$  is specified by the identity  $\psi(z_s) = \int_0^1 u(z)\phi_0(z) dz$ .

**Proof** The formula for  $z_s$  is derived from conservation of volume as follows. Integrating the PDE (3.1) over  $0 < z < 1$ , we obtain

$$\frac{d}{dx} \int_0^1 u(z)\phi(x, z) dz = \int_0^1 \frac{\partial}{\partial z} (\phi(1 - \phi)) dz = 0.$$

Thus,

$$\int_0^1 u(z)\phi_0(z) dz = \int_0^1 u(z)\phi(0, z) dz = \int_0^1 u(z)\phi(x, z) dz = \psi(z_s), \quad x \geq x_s,$$

the final equality following from (3.6) and the definition (2.2) of  $\psi$ .

To estimate  $x_s$ , we use the Lax formula [19] for the inviscid Burgers equation (3.3). Consider initial data  $v_1 : [0, 1] \rightarrow [-1, 1]$  given by an integrable function and extend  $v_1$  to

the real line by  $v_I(\zeta) = 1, \zeta < 0, v_I(\zeta) = -1, \zeta > 1$ . Then the initial value problem

$$v_\tau + v v_\zeta = 0, \quad -\infty < \zeta < \infty, \tau > 0 \quad (3.7)$$

with initial condition

$$v(\zeta, 0) = v_I(\zeta), \quad -\infty < \zeta < \infty \quad (3.8)$$

has a unique weak solution  $v$  with  $-1 \leq v(\zeta, \tau) \leq 1$  satisfying the entropy condition [19, 27] that includes the Lax condition (3.5) at shock waves. We wish to show that for all  $\tau \geq 2$ ,

$$v(\zeta, \tau) = \begin{cases} 1, & \zeta < \zeta_0 \\ -1, & \zeta > \zeta_0, \end{cases} \quad (3.9)$$

where  $\zeta_0 \in [0, 1]$  is defined by the conservation law:

$$\int_0^1 v(\zeta, \tau) d\zeta = 2\zeta_0 - 1 = \int_0^1 v_I(\zeta) d\zeta. \quad (3.10)$$

We refer to the formula (3.9), (3.10) as the *segregated solution*. In the transformed coordinates,  $\tau = 2$  corresponds to the maximum distance to segregation  $x = 2\psi(1)$  predicted in the theorem.

The Lax formula states that the entropy weak solution  $v = v(\zeta, t)$  is (almost everywhere in  $\zeta, \tau$ ) the minimiser of the function

$$\frac{1}{2}v^2\tau + \Phi(\zeta - v\tau), \quad \Phi(\eta) = \int_0^\eta v_I(\zeta) d\zeta. \quad (3.11)$$

The proof will be complete if we show that the segregated solution (3.9) minimises the function (3.11) at  $\tau = 2$ , i.e.,

$$v^2 + \Phi(\zeta - 2v) \geq \begin{cases} 1 + \Phi(\zeta - 2), & \zeta < \zeta_0 \\ 1 + \Phi(\zeta + 2), & \zeta > \zeta_0 \end{cases} \quad \text{for all } v \in \mathbb{R}, \quad (3.12)$$

with equality achieved only at (3.9). First, we calculate

$$\Phi(\zeta) = \begin{cases} \zeta, & \zeta < 0 \\ \int_0^\zeta v_I(\xi) d\xi, & 0 < \zeta < 1 \\ \Phi(1) + 1 - \zeta, & \zeta > 1. \end{cases} \quad (3.13)$$

Consequently, since  $\zeta - 2 < 0$  for  $\zeta < \zeta_0$ , and  $\zeta + 2 > 1$  for  $\zeta_0 < \zeta$ ,

$$1 + \Phi(\zeta - 2) = \zeta - 1, \text{ for } 0 \leq \zeta < \zeta_0; \quad 1 + \Phi(\zeta + 2) = \Phi(1) - \zeta, \text{ for } \zeta > \zeta_0. \quad (3.14)$$

Now consider  $v^2 + \Phi(\zeta - 2v)$  as a function of  $v$ , for fixed  $\zeta \in [0, 1]$ :

$$v^2 + \Phi(\zeta - 2v) = \begin{cases} \zeta - 2v + v^2, & v > \zeta/2 \\ \int_0^{\zeta-2v} v_1(\xi) d\xi + v^2, & \frac{1}{2}(\zeta - 1) < v < \frac{1}{2}\zeta \\ \Phi(1) + 1 - \zeta + 2v + v^2, & v < \frac{1}{2}(\zeta - 1). \end{cases} \quad (3.15)$$

We proceed by first showing (3.12) for the outside ranges for  $v$ . Consider  $v > \zeta/2$ . Then  $v^2 + \Phi(\zeta - 2v) = \zeta - 2v + v^2 \geq \zeta - 1$  collapses to  $(1 - v)^2 \geq 0$ , so that  $v^2 + \Phi(\zeta - 2v) \geq 1 + \Phi(\zeta - 2)$  for  $\zeta < \zeta_0$  (by (3.14)) in the range  $v > \zeta/2$ , with equality achieved at the expected solution  $v = 1$ . Similarly, for  $\zeta > \zeta_0$ , the inequality  $v^2 + \Phi(\zeta - 2v) \geq 1 + \Phi(\zeta + 2)$  becomes  $2(\zeta - \zeta_0) \geq 0$ , using  $\Phi(1) = 2\zeta_0 - 1$ , with equality achieved at no value of  $v$ .

Now consider  $v < \frac{1}{2}(\zeta - 1)$ , the other outside range for  $v$ . Then  $v^2 + \Phi(\zeta - 2v) = \Phi(1) + 1 - \zeta + 2v + v^2$ , and again it is straightforward to show (3.12) by considering the two ranges for  $\zeta$  separately. For  $\zeta < \zeta_0$ , the inequality collapses to  $2(\zeta_0 - \zeta) + (v + 1)^2 > 0$ , while for  $\zeta > \zeta_0$ , the inequality collapses to  $(v + 1)^2 \geq 0$ , with equality only at  $v = -1$ .

It remains to prove (3.12), with strict inequality, for  $v$  in the middle range  $\frac{1}{2}(\zeta - 1) < v < \zeta/2$ . Here, we have less precise information, due to the integral in (3.15). However, the following Lemma gives us the estimate we need.

**Lemma 1** *Let  $G : [a, b] \rightarrow \mathbb{R}$  be differentiable and satisfy, for some numbers  $A, B, m > 0$ :*

$$G(a) = A, \quad G(b) = B, \quad |G'(v)| \leq m \text{ for all } v \in [a, b].$$

Then,

$$\max\{A - m(v - a), B + m(v - b)\} \leq G(v) \leq \min\{A + m(v - a), B - m(v - b)\} \text{ for all } v \in [a, b]. \quad (3.16)$$

**Proof**  $G(v) = A + \int_a^v G'(\xi) d\xi \leq A + m(v - a)$ , for  $v \geq a$ , and  $G(v) = B - \int_v^b G'(\xi) d\xi \leq B - m(v - b)$ , for  $v \leq b$ . This proves the upper bound. The lower bound is proved similarly.

Now let

$$G(v) = \int_0^{\zeta-2v} v_1(\xi) d\xi, \quad \frac{1}{2}(\zeta - 1) < v < \frac{1}{2}\zeta,$$

regarding  $\zeta$  as a parameter. Then  $G(\frac{1}{2}(\zeta - 1)) = \Phi(1) = 2\zeta_0 - 1$ , and  $G(\frac{1}{2}\zeta) = 0$ . Moreover,  $G'(v) = -2v_1(\zeta - 2v)$ , so that  $|G'(v)| \leq 2$ . Applying the lemma with

$$a = \frac{1}{2}(\zeta - 1), \quad b = \frac{1}{2}\zeta, \quad A = \Phi(1), \quad B = 0, \quad m = 2,$$

we have

$$G(v) \geq \max\{2v - \zeta, -2v + \zeta + 2\zeta_0 - 2\} \geq \zeta_0 - 1, \quad (3.17)$$

since the minimum with respect to  $v$  is achieved at  $v = \frac{1}{2}(\zeta + \zeta_0 - 1)$ . Therefore, since

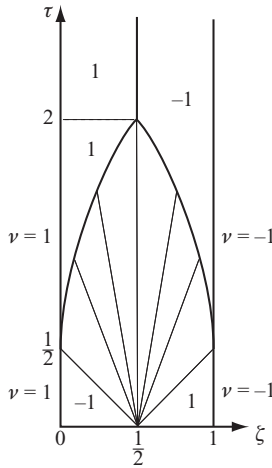


FIGURE 2. Solution with maximum distance to full segregation.

$G(v) = \Phi(\zeta - 2v)$ , we have

$$v^2 + \Phi(\zeta - 2v) \geq \zeta_0 - 1 \quad \text{for all } v.$$

To prove (3.12), we use (3.14) and observe that

$$\zeta_0 - 1 > \zeta - 1 = 1 + \Phi(\zeta - 2), \quad \text{for } 0 \leq \zeta < \zeta_0; \quad \zeta_0 - 1 > 2\zeta_0 - 1 - \zeta = 1 + \Phi(\zeta + 2), \quad \text{for } \zeta > \zeta_0.$$

This completes the proof of inequality (3.12), and hence completes the proof of the theorem.  $\square$

**Remarks:** 1. The upper bound  $x_s = 2\psi(1)$  for full segregation is sharp, since there is a solution that achieves segregation at this value. In the variables  $\zeta, \tau, v$  of the proof, this solution is shown in Figure 2. The rarefaction wave shown is  $u(\zeta, \tau) = \frac{\zeta - 1/2}{\tau}$ , and the shock on the left, calculated from the Rankine–Hugoniot condition, is given by

$$\zeta = \tau + 1/2 - \sqrt{2\tau}, \quad \tau > 1/2.$$

The solution is symmetric about  $\zeta = 1/2$ , so the shock on the right is  $\zeta = -\tau + 1/2 + \sqrt{2\tau}$ ,  $\tau > 1/2$ . A physical interpretation of this and similar solutions is given in [30].

2. It is worth comparing this result with estimates by Savage and Lun [26]. In their paper, Savage and Lun found an approximate solution for a steady and uniform inflow; that is, for  $\phi_0$  constant, assuming a linear velocity profile  $u(z) = \gamma z$ . The solution in that case consists of a pair of shock waves marking the boundaries between all large particles (at the top), all small particles (at the bottom) and the middle region, in which  $\phi = \phi_0$ . The point of complete segregation in this special case occurs at  $x_s = \frac{1}{2}\gamma$ , where the two shock waves meet, and merge into a single horizontal shock  $z = z_s = \sqrt{\phi_0}$ . Savage and Lun remark that it would be interesting to investigate the effects of a more general velocity profile on the segregation process. The transformation into Burgers equation shows that the velocity profile sets the vertical variable and does not affect the horizontal variable  $x$ ,

except through the factor  $\psi(1)$ , which can be scaled from the problem, so we take  $\psi(1) = 1$ . Consequently, the point  $x = x_s$ , where the steady flow is first completely segregated, is independent of the velocity profile, and depends only on the inflow. The vertical location  $z = z_s$  of the line separating the two layers downstream of  $x = x_s$  depends on both the velocity profile and the inflow mixture, and is given in Theorem 3.2 for an arbitrary inflow distribution, not only a uniform distribution.

#### 4 Dynamic shock waves

Discontinuities in  $\phi$  at time  $t = 0$  can propagate either as discontinuities, or as expansion fans, such as the equilibrium rarefaction wave mentioned above. Since equation (1.3) is in conservation form, we can write the Rankine–Hugoniot condition that relates the normal speed of a shock wave to the jump in  $\phi$  and the flux of  $\phi$  across the wave.

Consider a discontinuity located along the space-time surface  $z = z(x, t)$ , with normal  $\mathbf{N} = (z_t, z_x, -1)$ . The (space-time) divergence theorem applied to equation (1.3) yields the relation

$$z_t[\phi] + u(z)z_x[\phi] + [\phi(1 - \phi)] = 0, \quad (4.1)$$

in which square brackets indicate the jump, i.e., the difference between left- and right-hand limits:  $[f] = f_+ - f_-$ . Let  $\phi_\pm$  denote the one-sided limits of  $\phi$ . Dividing by  $[\phi]$ , equation (4.1) becomes

$$z_t + u(z)z_x = \phi_+ + \phi_- - 1. \quad (4.2)$$

When  $\phi_\pm$  are specified functions of  $(x, z, t)$ , this is an equation for the free boundary  $z = z(x, t)$ . The equation is quasi-linear in general (except for the plug-flow case in which  $u$  is constant, for example,  $\alpha = 1, u(z) = 1$  in (1.6)), and has a source term (the right-hand side). In simulations, we always find that sharp interfaces are stable when a mixture with larger particles is above a mixture with smaller particles, a property we can prove when the shock curve is *smooth*, i.e., continuously differentiable. Suppose  $\phi(x, z, t)$  has one-sided limits at the shock curve and define them by  $\phi_\pm(x, t) = \phi(x, z(x, t)_\pm, t)$ .

**Theorem 4.1** *A smooth shock wave is dynamically stable if*

$$\phi_+ < \phi_-. \quad (4.3)$$

**Proof** Consider a shock wave given by a curve  $z = \hat{z}(x, t)$ . Then the normal in space is  $\frac{1}{\sqrt{1+\hat{z}_x^2}}(-\hat{z}_x, 1)$ . We claim that condition (4.3) is the *Lax entropy condition* [19], which requires that characteristics approach the shock wave in forward time. To see this, we calculate the normal velocity of the shock and compare with the normal component of the speed of characteristics on either side, leading to the condition that characteristics impinge on the shock from both sides:

$$-u(z)\hat{z}_x + 2\phi_+ - 1 < -u(z)\hat{z}_x + \phi_+ + \phi_- - 1 < -u(z)\hat{z}_x + 2\phi_- - 1. \quad (4.4)$$

The outer inequality gives (4.3) after cancellation.

Now the theory of conservation laws establishes that the shock is non-linearly stable ([27], p. 216). Consider a shock satisfying (4.3) at some initial time. Then the initial shock location satisfies (4.4). The solution on each side of the shock is propagated using characteristics. But by (4.4), the region covered by the characteristics has an overlap, at least for a short time, so that  $\phi_+$  and  $\phi_-$  are determined in the overlap region. Because of the Lax condition, the shock will lie in the overlap region as well. It is found by solving the initial value problem for equation (4.2), with initial data given by the initial shock location. The method of characteristics gives a continuously differentiable solution for short time, since the initial data are smooth.  $\square$

**Remarks:** 1. We can explain the theorem intuitively as follows. Since large particles move upwards, and small particles move downwards, when  $0 < \phi_+ < \phi_- < 1$ , we find that  $\phi_+$  decreases and  $\phi_-$  increases, thereby increasing the segregation. (When  $\phi_+ = 0$  initially, then it is unchanged in the evolution, and similarly if  $\phi_- = 1$ .) Consequently, it is intuitive that the interface remains in place, marking the boundary between two distinct mixtures. On the other hand, if  $\phi_+ > \phi_-$ , then large particles migrate into the region above the discontinuity, and small particles migrate down, creating a ‘mushy zone’ that interpolates  $\phi$  between  $\phi_-$  and  $\phi_+$ . This zone represents a rarefaction in the language of hyperbolic equations; it is a continuous solution. In the context of particle flow, it is a mixing zone, in which two layers with different mixtures tend to mix in a region that grows in size, provided  $\phi_+ > \phi_-$ .

2. When the flow is fully segregated across a shock wave, we have  $\phi_+ = 0, \phi_- = 1$ , so that the equation for the shock location  $z = \hat{z}(x, t)$  is

$$z_t + u(z)z_x = 0,$$

which is similar to the inviscid Burgers equation. In particular, if  $\frac{\partial}{\partial x} \hat{z} < 0$ , then the shock will break and become unstable (i.e., the strict inequality (4.3) is reversed). This explains the reappearance of dynamic rarefaction waves after the shock has been established across a non-horizontal interface. As it happens, this breaking does not appear in the two cases of Sections 5 and 6, but it is discussed in our earlier papers [6, 29]. The continuation of the solution after a shock breaks is discussed in [20].

Sometimes it is convenient to parameterise a shock with  $z$  rather than with  $x$ . Then, writing the shock location as  $x = x(z, t)$ , the jump conditions lead to the equation

$$x_t + (\phi_+ + \phi_- - 1)x_z = u(z), \quad (4.5)$$

which has the virtue of being linear when the one-sided limits  $\phi_{\pm}$  are independent of  $x$ .

## 5 Case I

For the remainder of the paper, in this and the following section, we focus on the explicit solution of the specific illustrative initial boundary value problems of Cases I and II. In these examples, there are parameters  $\alpha, \beta$  in Case I and  $\alpha, z_r$  in Case II.

To solve the initial boundary value problem in Case I, we consult the proposed structure in Figure 3.

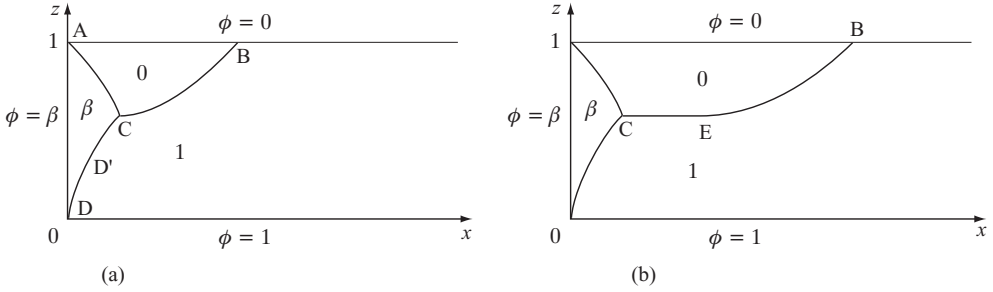


FIGURE 3. Case I (a) transient for small  $t$ , (b) long-time behaviour.

The particles in mixture  $\beta$  entering along  $x = 0$  form the region labelled with a  $\beta$ , bounded by the  $z$ -axis and curves  $AC$ , which will be stationary and  $CD$ , which turns out to be partly stationary (between  $D$  and  $D'$ ) and partly dynamic (i.e.,  $CD'$  is dependent on  $t$ ). The triple point  $C$  moves until at a time  $t = t^*$  it becomes stationary (and coincides with  $D'$ ). Thereafter, the pattern of discontinuities shown in Figure 3(b) applies, with a horizontal and stationary portion (labelled  $CE$ ) developing, while the curve  $BE$  moves to the right, without breaking, being extended by the shear flow.

To calculate the stationary curve  $AC$ , we solve equation (4.5) for the curve  $x = x_{AC}(z)$ , independent of  $t$  passing through  $x = 0, z = 1$ . In this equation,  $\phi_- = \beta, \phi_+ = 0$ , so the equation becomes

$$(\beta - 1) \frac{dx}{dz} = u(z), \quad x(1) = 0. \quad (5.1)$$

Integrating, and using (2.2), we obtain  $x$  as a function of  $z$ :

$$\text{AC:} \quad x = \frac{\psi(z) - \psi(1)}{(\beta - 1)}, \quad (5.2)$$

that is quadratic in the case of linear velocity profile, from (2.6).

To calculate the curve  $CD$ , we solve equation (4.5) for the function  $x = x(z, t)$ . Using  $\phi_- = \beta, \phi_+ = 1$ , we obtain the equation

$$x_t + \beta x_z = u(z), \quad (5.3)$$

with boundary and initial conditions

$$x(0, t) = 0, \quad t > 0, \quad x(z, 0) = 0, \quad 0 < z < 1. \quad (5.4)$$

This problem has a simple solution, since the right-hand side of (5.3) is independent of  $x$  and  $t$ :

$$\text{CD:} \quad x = x(z, t) = \begin{cases} \frac{\psi(z)}{\beta}, & 0 < z < \beta t, \\ \frac{1}{\beta}(\psi(z) - \psi(z - \beta t)), & z > \beta t. \end{cases} \quad (5.5)$$

Note that the two formulae match across the line  $z = \beta t$ , since  $\psi(0) = 0$ . The crossover at

$z = \beta t$  corresponds to the point D' in Figure 3(a), separating the time-dependent portion of the curve from the growing steady portion.

Now to locate C, we find the intersection of AC and CD, from equations (5.2) and (5.5):

$$\frac{1}{\beta}(\psi(z) - \psi(z - \beta t)) = \frac{\psi(z) - \psi(1)}{(\beta - 1)}. \quad (5.6)$$

For the linear velocity profile (1.6),  $\psi$  (given by (2.6)) is quadratic, so that equation (5.6) is quadratic in both  $z$  and  $t$ . Solving for  $z$ , we find

$$z = \tilde{z}(t) = \frac{1}{2}\{-(\alpha + 2(1 - \alpha)(1 - \beta)t) + [(\alpha - 2)^2 + 4^2(1 - \alpha)^2(1 - \beta)t^2]^{1/2}\}/(1 - \alpha), \quad (5.7)$$

the root with the property that  $z = 1$  when  $t = 0$ . Then C has coordinates  $(\tilde{x}(t), \tilde{z}(t))$ , with

$$\tilde{x}(t) = \frac{\psi(\tilde{z}(t)) - \psi(1)}{(\beta - 1)}. \quad (5.8)$$

Now D and C merge and then become stationary when  $\tilde{z}(t) = \beta t$  (see (5.5)). But substituting  $z = \beta t$  into (5.6), the equation reduces to

$$\psi(\beta t) = \beta\psi(1).$$

For the linear velocity profile (1.6), this gives a quadratic equation for  $t = t^*$ :

$$\alpha t + (1 - \alpha)\beta t^2 = 1,$$

with solution

$$t = t^* = \frac{-\alpha + \sqrt{(\alpha^2 + 4(1 - \alpha)\beta)}}{2(1 - \alpha)\beta}. \quad (5.9)$$

Finally, we compute the interfaces BC in Figure 3(a) and CEB in Figure 3(b). In both cases,  $\phi_+ = 1$ ,  $\phi_- = 0$ , leading to the PDE for  $z = z(x, t)$ :

$$z_t + u(z)z_x = 0, \quad (5.10)$$

and boundary condition

$$z(\tilde{x}(\tau), \tau) = \tilde{z}(\tau). \quad (5.11)$$

Thus, for each  $t < t^*$ ,

$$\text{BC: } x = u(\tilde{z}(\tau))(t - \tau) + \tilde{x}(\tau), \quad z = \tilde{z}(\tau), \quad 0 \leq \tau \leq t \leq t^*, \quad (5.12)$$

which is the curve BC of Figure 3(a) parameterised by  $\tau$ . For  $t \geq t^*$ , the section BE of the curve BEC is given by (5.12), for  $0 \leq \tau \leq t^*$ , but for  $t^* \leq \tau \leq t$ ,  $\tilde{x}(\tau) = \bar{x}$ ,  $\tilde{z}(\tau) = \bar{z}$  are constant, so that

$$\text{EC: } x = u(\bar{z})(t - \tau) + \bar{x}, \quad z = \bar{z}, \quad t < \tau < t^* \quad (5.13)$$

defines the horizontal line EC, parameterised by  $\tau$ . Note that the section BE is convected

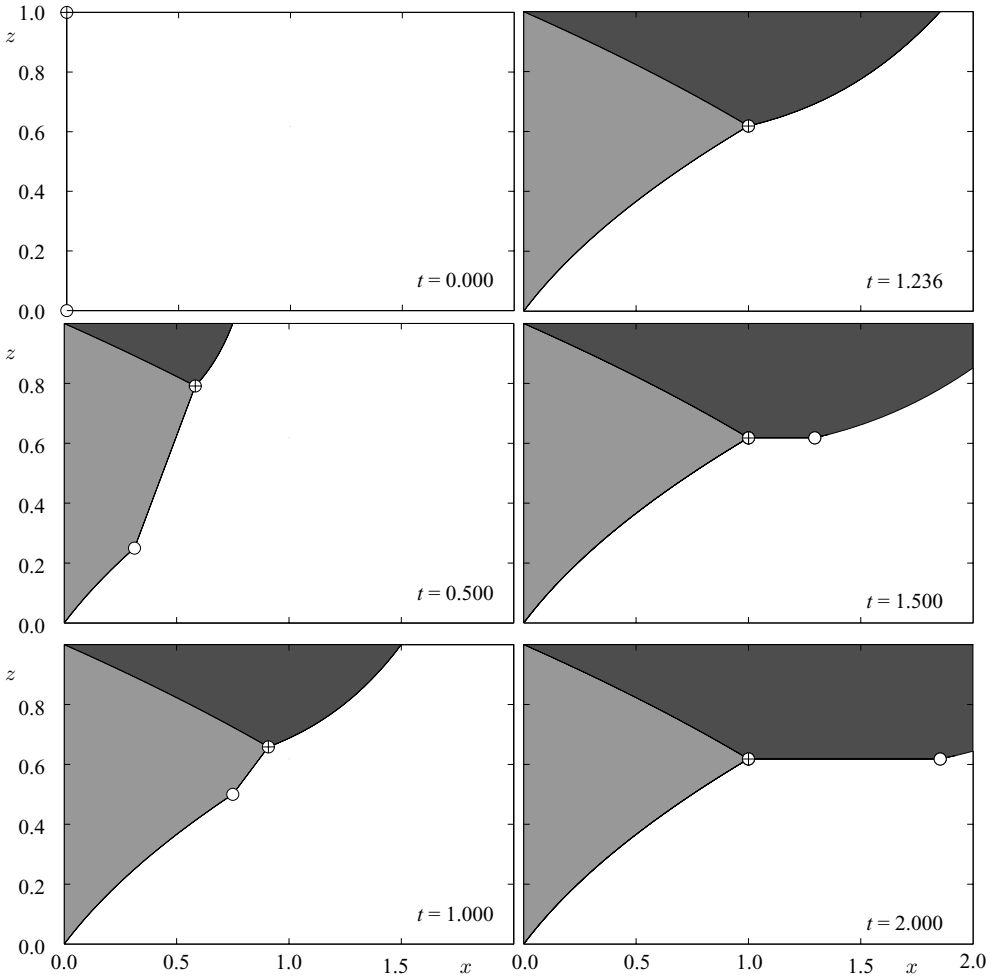


FIGURE 4. The evolution of the volume fraction of small particles  $\phi$  as a function of  $x$  and  $z$ . The particles enter the chute at  $x = 0$  and are swept downstream from left to right by a linear velocity field given by parameter  $\alpha = 0.5$ . The white region corresponds to 100% small particles, the dark region to 100% large particles and the light grey region to the mixed region with concentration  $\phi_0 = 0.5$ . The circular markers correspond to the position of the transition points and the ‘ $\oplus$ ’ is the triple-point.

to the right with speed  $u(z)$  without breaking, being extended by the shear flow, since for fixed  $\tau \in [0, t^*]$ ,  $z = \tilde{z}(\tau)$  is constant, but  $x$  grows linearly with  $t$ :

$$\text{BE:} \quad x = u(\tilde{z}(\tau))(t - \tau) + \tilde{x}(\tau), \quad z = \tilde{z}(\tau), \quad 0 \leq \tau \leq t^*, \quad t > t^*.$$

The various formulae for the curves have been programmed in MATLAB, which was used to generate snapshots of the evolution shown in Figure 4. In the figure, the points A, B, C, etc. (labelled in Figure 3) are shown as circles.

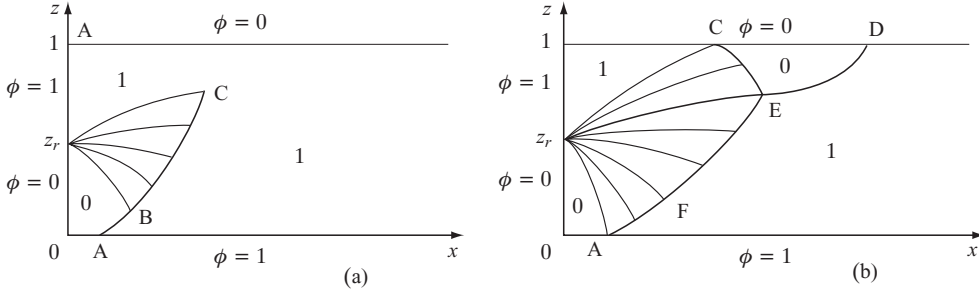


FIGURE 5. Case II (a) transient for small  $t$ , (b) intermediate time behaviour, before E and F collide.

## 6 Case II

In Case II, the inflow boundary condition is different, with all small particles above all large particles. This gives rise to a rarefaction fan centred at the dividing point, as shown in Figure 5(a). The fan propagates downstream, together with a region of all large particles, forming a shock wave labelled ABC in the figure. After the points B and C reach the lower and upper boundaries, they become anchored, as shown in Figure 5(b), and reflected dynamic shocks CE, AF are formed, with E and F approaching. Finally, E and F collide, at a time  $t = t_{\text{steady}}$ . The only moving boundary in the subsequent motion is a convected shock DE similar to the curve BE in Case I.

As for Case I, we can characterise the entire solution in the case of linear shear. This is encoded into a MATLAB program, which produces the evolution for specified parameters. In Figure 8 we show the evolution for representative values of  $z_r$  and  $\alpha$ .

The values of  $\phi = \phi_R(x, z)$  in the rarefaction wave are given by the explicit equation (2.4), in the time-independent case

$$\phi_R(x, z) = \frac{1}{2} \left( 1 + \frac{\psi(z) - \psi(z_r)}{x} \right). \quad (6.1)$$

The interface AB is a shock, and it is easy to calculate (and to justify physically) that it simply marks where inflowing particles are transported to after a given time  $t$ :

$$x = u(z)t. \quad (6.2)$$

The location of the point B is the intersection at time  $t$  of this curve with the fixed curve  $\phi = 0$  (i.e.,  $x = \psi(z_r) - \psi(z)$ ) from the rarefaction (6.1). Eliminating  $x$ , we obtain the equation

$$u(z)t = \psi(z_r) - \psi(z). \quad (6.3)$$

for the  $z$  coordinate  $z = z_B(t)$  of B. The  $x$  coordinate is then  $x = x_B(t) = u(z_B(t))t$  (from (6.2)). In the case of linear  $u(z)$ , we can solve the quadratic equation (6.3) explicitly for  $z = z_B(t)$ ; thus,

$$\begin{aligned} x_B(t) &= (\alpha + 2(1 - \alpha)z_B(t))t; \\ z_B(t) &= \frac{1}{2(1-\alpha)} \left( -(\alpha + 2t(1 - \alpha)) + \sqrt{(\alpha + 2t(1 - \alpha))^2 + 4(1 - \alpha)(\psi(z_r) - t\alpha)} \right). \end{aligned} \quad (6.4)$$

### The curve BC

The boundary BC is a truly dynamic two-dimensional shock, even though  $\phi$  is independent of time  $t$  on each side, and we need the entire equation (4.2) to determine it as a graph  $z = z_{BC}(x, t)$ . Part of this curve survives as EF in Figure 5(b) after the points B and C have reached the upper and lower boundaries and been reflected as points E and F.

In equation (4.2), we let  $\phi_+ = 1$ , and  $\phi_- = \phi_R(x, z)$ , given by (6.1). Thus,  $z = z_{BC}(x, t)$  satisfies

$$z_t + u(z)z_x = \frac{1}{2} \left( 1 + \frac{\psi(z) - \psi(z_r)}{x} \right). \quad (6.5)$$

In solving equation (6.5), we use the method of characteristics. Thus,

$$\frac{dx}{dt} = u(z); \quad \frac{dz}{dt} = \frac{1}{2} \left( 1 + \frac{\psi(z) - \psi(z_r)}{x} \right), \quad (6.6)$$

which gives  $z$  implicitly:

$$\psi(z) = \psi(z_r) + x + \lambda\sqrt{x}, \quad (6.7)$$

with a constant of integration  $\lambda$ . Characteristics in the  $(x, t)$ -plane emanate from the curve

$$x = x_B(\tau), \quad t = \tau, \quad 0 < \tau < \min(t, t_B), \quad (6.8)$$

on which  $z = z_B(\tau)$ , where the functions  $x_B, z_B$  are given by formulae (6.4). The constant  $t_B$  is the time at which  $B$  hits the  $x$ -axis  $z = 0$ :

$$t_B = \frac{\psi(z_r)}{\alpha}, \quad \text{for which} \quad x_B(t_B) = \psi(z_r), \quad z_B(t_B) = 0. \quad (6.9)$$

In the case of simple shear ( $\alpha = 0$ ) there is no slip along the bottom boundary and point A is pinned at  $x = 0$ . Correspondingly the time for the point B to reach the  $x$ -axis  $t_B \rightarrow \infty$  as  $\alpha \rightarrow 0$  as shown in Figure 6. Characteristics are found in the form of  $t$  as a function of  $x$ , with  $z$  as a function of  $x$  given by (6.7),  $\lambda$  labelling the characteristic. Thus, using  $\tau$  to parameterise the family of characteristics (i.e., the starting points), let us define the characteristics by  $(x, t = \hat{t}(x, \tau), z = \hat{z}(x, \tau))$ .

Then for fixed  $\tau$ , the side condition for (6.6) becomes

$$x = x_B(\tau), \quad t = \hat{t}(x_B, \tau) = \tau, \quad z = \hat{z}(x_B, \tau) = z_B(\tau). \quad (6.10)$$

This gives  $\lambda$  in formula (6.7):

$$\lambda = \lambda(\tau) = (\psi(z_B(\tau)) - \psi(z_r) - x_B(\tau)) / \sqrt{x_B(\tau)}, \quad (6.11)$$

thereby defining  $z = \hat{z}(x, \tau)$ , satisfying (6.7).

It remains to find  $t = \hat{t}(x, \tau)$ . Returning to the first equation in (6.6), we have, using (2.8),

$$\frac{dx}{dt} = u(z) = \sqrt{\alpha^2 + 4(1 - \alpha)\psi}. \quad (6.12)$$

But  $\psi$  can be substituted from (6.7) to express the right-hand side as a function of  $x$  and

$\tau$ , leading to the first integral

$$t = \int \frac{1}{\sqrt{a + bx + c\sqrt{x}}} dx + A, \quad (6.13)$$

where  $a = \alpha^2 + 4(1 - \alpha)\psi(z_r)$ ,  $b = 4(1 - \alpha)$ ,  $c = 4(1 - \alpha)\lambda$  and  $A$  is the constant of integration. Evaluating the integral, we find

$$t = \frac{2}{b} \sqrt{a + bx + c\sqrt{x}} - \frac{c}{b^{3/2}} \ln \left( \frac{c + 2b\sqrt{x}}{\sqrt{b}} + \sqrt{a + bx + c\sqrt{x}} \right) + A. \quad (6.14)$$

From the boundary conditions, we get an expression for  $A$ . Let  $F(x, \tau) + A$  denote the right-hand side of equation (6.14) (bearing in mind that  $c$  depends on  $\lambda = \lambda(\tau)$ .) Then the first and second boundary conditions in (6.10) give

$$A = A(\tau) = \tau - F(x_B, \tau). \quad (6.15)$$

Then  $t = \hat{t}(x, \tau) = \tau + F(x, \tau) - F(x_B(\tau), \tau)$ . Finally, we have the family of characteristic curves in  $x, t, z$ :

$$\{(x, t = \hat{t}(x, \tau), z = \hat{z}(x, \tau)) : x > x_B(\tau)\}, \quad 0 < \tau < \min(t, t_B). \quad (6.16)$$

Now to complete the solution, and obtain the curve BC at each time  $t$ , we have to solve the equation

$$t = \hat{t}(x, \tau), \quad x \geq x_B(\tau), \quad 0 < \tau < \min(t, t_B), \quad (6.17)$$

to get a function  $\tau = \tilde{\tau}(t, x)$ . Then the curves we seek for given  $t > 0$  are

$$\text{BC: } \{(x, z = \hat{z}(x, \tilde{\tau}(t, x))) : x > x_B(t)\}. \quad (6.18)$$

The point C first reaches the upper boundary at a time  $t_C$  at the value of  $x$  for which  $z = 1$  on the curve  $\phi = 1$ , leading to

$$x = \bar{x}_C = 1 - \psi(z_r). \quad (6.19)$$

## Lemma 2

$$t_C = 1 - z_r \quad (6.20)$$

**Proof** On BC,  $x$  and  $z$  are related by (6.7), with  $\lambda = \lambda(\tau)$  given by (6.11). Substituting (6.19) into (6.7), we find  $\lambda\sqrt{x_C} = 0$ , from which we deduce that  $\lambda(\tau) = 0$ . This makes sense because the point C lies on the characteristic labelled by  $\tau = 0$  (or  $\lambda = 0$ ), emanating from the point  $(x, z, t) = (0, z_r, 0)$ , since  $z_r = z_B(0)$ .

Setting  $\tau = 0$  in (6.18), and observing that  $c = 0$ , since  $\lambda = 0$ , we find  $t = \hat{t}(x, 0) = \frac{2}{b}(\sqrt{a + bx} - \sqrt{a})$  (from which we can obtain  $x$  as a function of  $t$  at the point C). Substituting  $x = \bar{x}_C$  from (6.19) and the forms for the constants  $a, b$ , we are led to the formula (6.20), after applying (2.8). The proof is complete.  $\square$

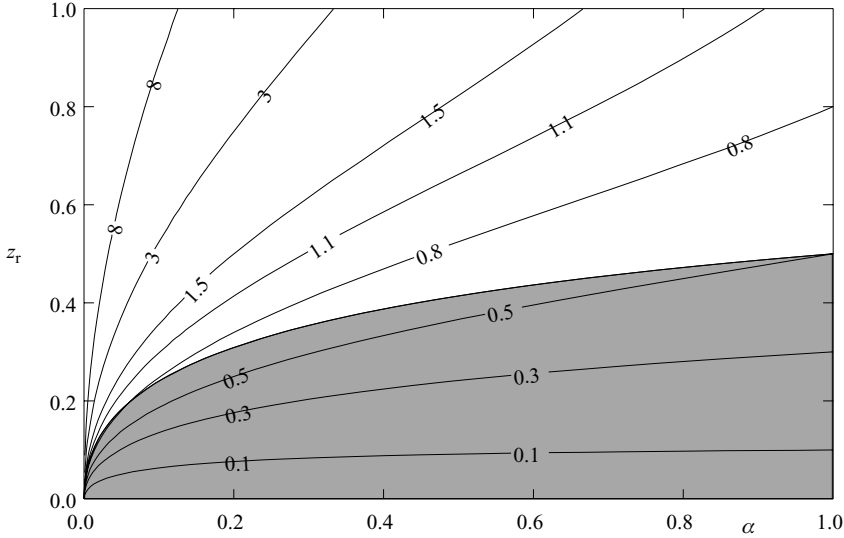


FIGURE 6. A contour plot of the time  $t_B$  for the lead characteristic to reach the bottom of the flow, as a function of  $z_r$  and  $\alpha$ . The shaded region is the range of parameters for which the fan hits the base before the surface.

In Figure 6, we show contours of the time  $t_B = t_B(\alpha, z_r)$  at which the rarefaction fan first hits the lower boundary  $z = 0$ . From (6.9), these are easily calculated to be

$$\alpha = \frac{z_r^2}{z_r^2 - z_r + t_B}.$$

Also shown is the locus of parameters on which  $t_B$  coincides with the time  $t_C$  at which the rarefaction fan first hits the upper boundary  $z = 1$ . This is the parabola obtained by equating the expressions in (6.9) and (6.20).

Now let us turn to the structure of the solution at later times, shown in Figure 5(b). The points E and F and the curve DE result from the reflection of waves from the boundaries  $z = 0$  and  $z = 1$ . As remarked earlier, the section EF has the same parameterisation (5.12) as the curve BC in Figure 5(a). The point A remains fixed; whereas for earlier times it was swept forward by the motion of large particles along the boundary, these particles are now displaced from the boundary at A, and replaced by small particles that cross the curve AF, which is also stationary. Thus, the point F tracks along the edge of the stationary rarefaction, connecting a stationary shock AF to the shock EF, which is still moving, until F and E collide. Similarly, the point E marks the end of a stationary shock CE. From this point, a second dynamic shock DE opens up, with D being swept along the boundary by large particles. Finally, after E and F collide, the curve DE develops a horizontal stationary shock  $z = z_S$  whose left end point is the now stationary point  $E = F$ .

The locus of F for  $t > t_B$  can be described using explicit constructions. Since AF is stationary, we have  $u(z)z_x = \frac{1}{2}(1 + \frac{\psi(z)-\psi(z_r)}{x})$ , leading to (as for dynamic shocks)

$$\psi(z) = x + \psi(z_r) + \lambda\sqrt{x}. \quad (6.21)$$

To determine the constant of integration  $\lambda$ , observe that  $z = 0$  at  $x = x_A = \psi(z_r)$ . Thus,  $\lambda = -2\sqrt{\psi(z_r)}$ , so that

$$\text{AF:} \quad \psi(z) = x + \psi(z_r) - 2\sqrt{\psi(z_r)x}. \quad (6.22)$$

From this formula and  $\psi'(0) = u(0) = \alpha$ , we deduce that, for  $\alpha > 0$ , the curve AF has a horizontal tangent at A:

$$\frac{dz}{dx} = 0 \quad \text{at A.}$$

Now for the locus of F =  $(x_F(t), z_F(t))$ . At this point, we have  $t = \hat{t}(x_F(t), \tau), z_F(t) = \hat{z}(x_F(t), \tau)$ , with  $\tau \leq t_B$ , where  $\hat{t}, \hat{z}$  are given by (6.7), (6.11), (6.14). But we also know that  $(x_F(t), z_F(t))$  lies on AF, so it satisfies (6.22). Comparing (6.7), (6.22), we find  $\lambda(\tau) = -2\sqrt{\psi(z_r)}$ , the same value as for the entire curve AF. But from (6.9) and (6.11), we see that this specifies  $\tau = t_B$ . The point F is given by determining  $x_F(t)$  as a function of  $t$  from the implicit equation

$$\hat{t}(x_F(t), t_B) = t. \quad (6.23)$$

Similarly, the curve CE is stationary, hence  $u(z)z_x = \frac{1}{2}(\frac{\psi(z)-\psi(z_r)}{x} - 1)$ , giving  $\psi(z) = -x + \psi(z_r) + \lambda\sqrt{x}$ , with  $\lambda$  given by  $\lambda = 2\sqrt{1 - \psi(z_r)}$ . Consequently,

$$\text{CE:} \quad \psi(z) = -x + \psi(z_r) + 2\sqrt{(1 - \psi(z_r))x}. \quad (6.24)$$

The locus of the shock DE depends on the location  $(x_E(t_o), z_E(t_o))$  of the point E, before E and F collide at time  $t_{\text{steady}}$ . Thus,  $t_C \leq t_o \leq t$ , for  $t_C < t < t_{\text{steady}}$ , and

$$\text{DE:} \quad x = x_E(t_o) + u(z_E(t_o))(t - t_o), \quad z = z_E(t_o). \quad (6.25)$$

The point at which E and F collide, also labelled E =  $(x_E, z_E)$  in Figure 5(b), lies on both AF, given by equation (6.22) and CE, given by equation (6.24), so that

$$x_E = (\sqrt{1 - \psi(z_r)} + \sqrt{\psi(z_r)})^2, \quad \psi(z_E) = 1 - \psi(z_r). \quad (6.26)$$

We note that  $z_E$  satisfies the requirement of conservation of mass for steady flow (Theorem 3.2). Since  $x_F(t) = x_E$  at  $t = t_{\text{steady}}$ , equation (6.23) is a formula for

$$t_{\text{steady}} = \hat{t}(x_E, t_B), \quad (6.27)$$

where both  $x_E$  (given by (6.26)) and  $t_B$  (given by (6.9)) depend only on  $z_r, \alpha$ . Contours of the function  $t_{\text{steady}}(z_r, \alpha)$  are plotted in Figure 7. The solution in Case II is plotted in Figure 8, where we show the evolution of the solution according to the formulae in this section. The points labelled A, B, C, etc. in Figure 5 are shown as circles in Figure 8.

The derivation of equation (6.27) takes the same form as equation (5.54) in the earlier paper [6]. The essential difference lies in the fact that the time  $t_B$  for the rarefaction fan

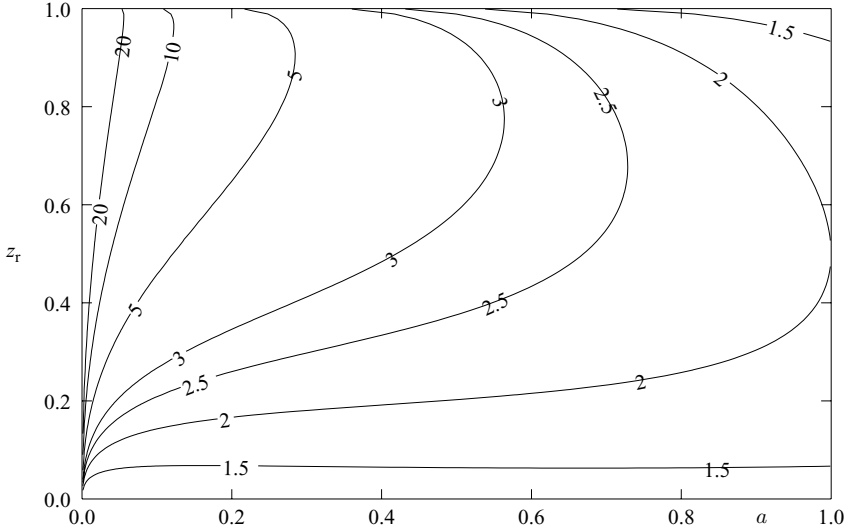


FIGURE 7. A contour plot of the time  $t_{\text{steady}}$  for the fan region to reach steady-state, as a function of  $z_r$  and  $\alpha$ .

to impinge on the bottom boundary is different in the two calculations. In both cases, in the limit  $\alpha \rightarrow 0$  there is no slip along the basal boundary and the rarefaction fan does not attain a steady state in finite time. This manifests itself as a logarithmic singularity in  $t_{\text{steady}}$  as  $\alpha \rightarrow 0$ , as was discussed in detail in Section 5(d) of [6].

The limit  $\alpha \rightarrow 0$  is of physical relevance for avalanche flows over rough beds where there is no slip at the base, e.g., in Savage and Lun's experiments [26]. When  $\alpha = 0$ , the solution in Case II has the property that the base of the rarefaction wave centred at  $x = 0$ ,  $z = z_r$  does not reach the base  $z = 0$  in finite time. A physical explanation is that for  $\alpha = 0$ , the small particles adjacent to the base cannot move, either horizontally (since  $u(0) = 0$ ) or vertically (since there are no other particles to displace them). Moreover, the steady shock separating large from small particles and emerging from the base is in fact pinned at the origin when  $\alpha = 0$ . This corresponds to the transition from large incoming particles to small particles along the base.

In a similar problem considered in [6], there is an interestingly different behaviour. In that case, the initial condition has all large particles adjacent to the base, and the rarefaction wave reaches the base in finite time, displacing the large particles and creating a layer of small particles. The larger particles have a positive vertical velocity as soon as the rarefaction reaches them. In this case, the transition from large to small particles along the base occurs at the point  $x > 0$  at which the rarefaction first reaches the base. Moreover, as in Case II of the paper, this point is pinned.

## 7 Conclusions

The Gray and Thornton [8] and Thornton *et al.* [30] models for particle-size segregation both consist of a scalar conservation law in two space dimensions and time. The equation

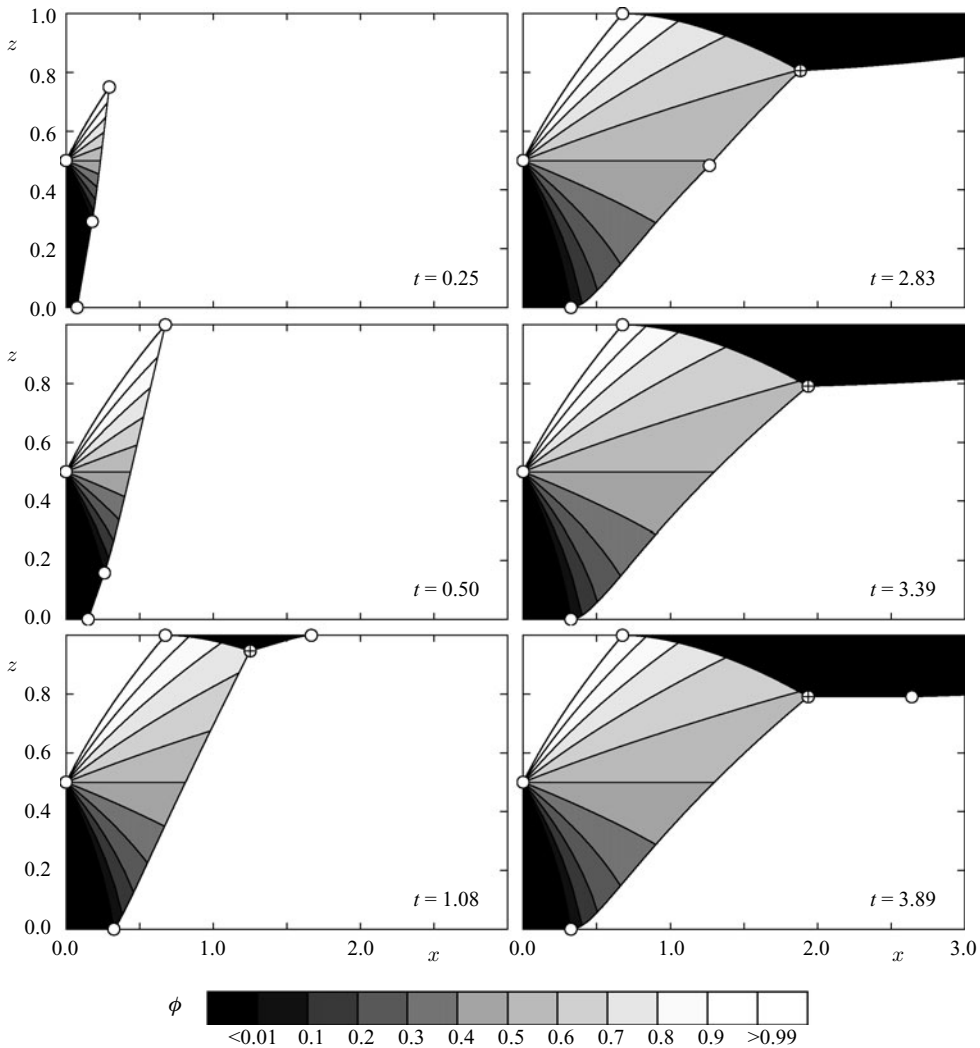


FIGURE 8. A series of contour plots showing the evolution of the volume fraction of small particles  $\phi$  as a function of the downstream coordinate  $x$  and avalanche depth  $z$ . The bulk linear shear flow is from left to right and is given by parameter  $\alpha = 0.3$ . The normally graded particles enter the chute at  $x = 0$  and have a concentration discontinuity at  $z_r = 0.5$ . The white circular markers show the position of the key steady and unsteady points in the flow and the triple-point is shown with an ‘ $\oplus$ ’.

has non-constant coefficients, but these appear only in the component of flux that is linear in the dependent variable  $\phi$ . The other component, measuring vertical segregation, is quadratic in  $\phi$ , but has a constant segregation rate. One possible generalisation of the model would be to allow the segregation rate to depend on the shear rate, since this would make sense physically if segregation is driven primarily by shear rate. However, in this paper, we consider only the simpler situation in which the shear rate is constant, so that the segregation rate is also constant in space and time. We explore properties of

the model from the theoretical point of view of non-linear PDE, specifically non-linear conservation laws, interpreting the results in terms of the physical variables. The two main results are (i) a characterization of stable shocks, corresponding to interfaces separating two different mixtures of large and small particles; stability requires that there is a greater concentration of small particles below the shock than above and (ii) a sharp estimate of the distance from a steady inflow boundary to where the resulting steady flow is fully segregated into a layer of large particles above a layer of small particles. For dynamic problems, we calculate explicit solutions in two physically significant cases, showing how stationary shocks and rarefactions fit together with dynamic stable shocks to generate the solution.

Since the conservation law is posed in an unbounded domain, but with both no-flux and inflow boundary conditions, standard existence and uniqueness theory for scalar equations does not apply. Nonetheless, we expect that the theory developed by Kruzkov, and more recently by others [18, 27], can be adapted to segregation models with the full range of boundary conditions (i.e., inflow mixtures depending on both depth  $z$  and time  $t$ ) suggested by the context of avalanche flow.

The solutions in this paper have been constructed for a uniform thickness avalanche and a prescribed velocity field. In general, both  $h$  and  $\mathbf{u}$  evolve in space and time as the avalanche flows downslope. A natural next step will be to couple the segregation model discussed in this paper to existing avalanche models (e.g., [4, 7, 9, 12, 25, 31]). Such a coupled model has the potential to quantify our understanding of some of the subtle size-mobility feedbacks that lead to the spontaneous formation of coarse-grained lateral levees in debris and pyroclastic flows [13, 14, 22, 23]. This could be accomplished by solving the avalanche model for the thickness  $h$  and depth-averaged velocity  $\bar{\mathbf{u}}$ , reconstructing the three-dimensional velocity  $\mathbf{u}$  using incompressibility and assumed flow profiles with depth and then using (1.1) to compute the concentration  $\phi$ . A full coupling can then be achieved by making the basal sliding friction dependent on the local concentration of small particles. The uncoupled problems presented in this paper provide important test cases for more general coupled solutions.

### Acknowledgements

The research of MS was supported by the U.S. National Science Foundation through grants DMS 0244488 and DMS 0604047. JMNTG also gratefully acknowledges the support of an EPSRC Advanced Research Fellowship (GR/S50052/01 and GR/S50069/01) as well as MIMS support from the School of Mathematics at the University of Manchester.

### References

- [1] BAGNOLD, R. A. (1954) Experiments on a gravity-free dispersion of large spheres in a Newtonian fluid under shear. *Proc. R. Soc. Lond. A* 255, 49–63.
- [2] DOLGUNIN, V. N. & UKOLOV, A. A. (1995) Segregation modelling of particle rapid gravity flow. *Powder Technol.* 83, 95–103.
- [3] GRAY, J. M. N. T. & CHUGUNOV, V. A. (2006) Particle-size segregation and diffusive remixing in shallow granular avalanches. *J. Fluid Mech.* 569, 365–398.

- [4] GRAY, J. M. N. T. & CUI, X. (2007) Weak, strong and detached oblique shocks in gravity driven granular free-surface flows. *J. Fluid Mech.* 579, 113–136.
- [5] GRAY, J. M. N. T. & HUTTER, K. (1997) Pattern formation in granular avalanches. *Contin. Mech. Thermodyn.* 9, 341–345.
- [6] GRAY, J. M. N. T., SHEARER, M. & THORNTON, A. R. (2006) Time-dependent solutions for particle-size segregation in shallow granular avalanches. *Proc. R. Soc. A* 462, 947–972.
- [7] GRAY, J. M. N. T., TAI, Y.-C. & NOELLE, S. (2003) Shock waves, dead-zones and particle-free regions in rapid granular free surface flows. *J. Fluid Mech.* 491, 161–181.
- [8] GRAY, J. M. N. T. & THORNTON, A. R. (2005) A theory for particle size segregation in shallow granular free-surface flows. *Proc. R. Soc.* 461, 1447–1473.
- [9] GRAY, J. M. N. T., WIELAND, M. & HUTTER, K. (1999) Free surface flow of cohesionless granular avalanches over complex basal topography. *Proc. R. Soc. A* 455, 1841–1874.
- [10] HILL, K. M., KHARKAR, D. V., GILCHRIST, J. F., MCCARTHY, J. J. & OTTINO, J. M. (1999) Segregation driven organization in chaotic granular flows. *Proc. Natl. Acad. Sci. USA* 96, 11689–12210.
- [11] HUTTER, K. & KOCH, T. (1991) Motion of a granular avalanche in an exponentially curved chute: Experiments and theoretical predictions. *Phil. Trans. R. Soc. Lond. A* 334, 93–138.
- [12] IVERSON, R. M. (1997) The physics of debris flows. *Rev. Geophys.* 35, 245–296.
- [13] IVERSON, R. M. (2003) The debris-flow rheology myth. In: D. Rickenmann & C. L. Chen (editors), *Debris-Flow Hazards Mitigation: Mechanics, Prediction and Assessment* Millpress, Rotterdam, pp. 303–314.
- [14] IVERSON, R. M. & VALLANCE, J. W. (2001) New views of granular mass flows. *Geology* 29, 115–118.
- [15] JAYNES, E. T. (1963) Information theory and statistical mechanics. In: K. W. Ford (editor), *Statistical Physics III*. Benjamin, N.Y., pp. 181–218.
- [16] KHAKHAR, D. V., MCCARTHY, J. J. & OTTINO, J. M. (1997) Radial segregation of granular mixtures in rotating cylinders. *Phys. Fluids* 9, 3600–3614.
- [17] KHAKHAR, D. V., MCCARTHY, J. J. & OTTINO, J. M. (1999) Mixing and segregation of granular materials in chute flows. *Chaos* 9, 594–610.
- [18] KRUŽKOV, S. N. (1970) First order quasilinear equations in several independent variables. *Mat. Sb.* 81, 217–243.
- [19] LAX, P. D. (1957) Hyperbolic systems of conservation laws II. *Comm. Pure Appl. Math.* 10, 537–566.
- [20] MCINTYRE, M., ROWE, E., THORNTON, A. R., GRAY, J. M. N. T. & SHEARER, M. (2008) A lens-shaped mixing zone in granular avalanches with particle-size segregation. *AMRX*, Vol. 2008, Article ID abm008, 12 pages, doi:10.1093/amrx/abm008.
- [21] MIDDLETON, G. V. & HAMPTON, M. A. (1976) Subaqueous sediment transport and deposition by sediment gravity flows. In: D. J. Stanley & D. J. P. Swift (editors), *Marine Sediment Transport and Environmental Management*, Wiley, N.Y. pp. 197–218.
- [22] PHILLIPS, J. C., HOGG, A. J., KERSWELL, R. R. & THOMAS, N. H. (2006) Enhanced mobility of granular mixtures of fine and coarse particles. *Earth Planet. Sci. Lett.* 246, 466–480.
- [23] POULIQUEN, O., DELOUR, J. & SAVAGE, S. B. (1997) Fingering in granular flows. *Nature*, 386, 816–817.
- [24] POULIQUEN, O. & VALLANCE, J. W. (1999) Segregation induced instabilities of granular fronts. *Chaos* 9, 621–630.
- [25] SAVAGE, S. B. & HUTTER, K. (1989) The motion of a finite mass of granular material down a rough incline. *J. Fluid Mech.* 199, 177–215.
- [26] SAVAGE, S. B. & LUN, C. K. K. (1988) Particle size segregation in inclined chute flow of dry cohesionless granular solids. *J. Fluid Mech.* 189, 311–335.
- [27] SERRE, D. (2000) *Systems of Conservation Laws*, Vol. 2. Cambridge University Press. Cambridge, U.K.

- [28] SILBERT, L. E., ERTAS, D., GREST, G. S., HALEY, T. C. LEVINE, D. & PLIMPTON, S. J. (2001) Granular flow down an inclined plane: Bagnold scaling and rheology. *Phys. Rev. E* 64, 051302.
- [29] THORNTON, A. R. & GRAY, J. M. N. T. (2008) Breaking size-segregation waves and particle recirculation in granular avalanches. *J. Fluid Mech.* 596, 261–284.
- [30] THORNTON, A. R., GRAY, J. M. N. T. & HOGG, A. J. (2006) A three-phase mixture theory for particle size segregation in shallow granular free-surface flows. *J. Fluid. Mech.* 550, 1–25.
- [31] VALLANCE, J. W. (2000) Lahars. In: H. Sigurdsson, B. Houghton, S. R. McNutt, H. Rymer and J. Stix (editors), *Encyclopedia of Volcanoes*. Academic Press, New York, pp. 601–616.
- [32] VALLANCE, J. W. & SAVAGE, S. B. (2000) Particle segregation in granular flows down chutes. In: A. D. Rosato & D. L. Blackmore (editors), *IUTAM Symposium on Segregation in Granular Materials*. Kluwer Academic, Dordrecht, The Netherlands. pp. 31–51.
- [33] ZURIGUEL, I., GRAY, J. M. N. T., PEIXINHO, J. & MULLIN, T. (2006) Pattern selection by a granular wave in a rotating drum. *Phys. Rev. E* 73, 061302.